Nadezhda A. Slavinskaya, Uwe Riedel, Seth B. Dworkin, Murray J. Thomson

Detailed Numerical Modelling of PAH Formation and Growth in Non-Premixed Ethylene and Ethane Flames

Combustion and Flame, 2012,159, 979–995.

The original publication is available at www.elsevier.com
http://dx.doi.org/10.1016/j.combustflame.2011.10.005

Detailed Numerical Modelling of PAH Formation and Growth in Non-Premixed Ethylene and Ethane Flames

Nadezhda A. Slavinskaya, phone: +49 711 6862 543
Uwe Riedel, phone: +49-711-6862-351
Institute of Combustion Technology
German Aerospace Centre (DLR)
Pfaffenwaldring 38-40
70569, Stuttgart, Germany

Seth B. Dworkin, phone: 1 (416) 946-7743
Murray J. Thomson, phone: 1 (416) 580-3391
Department of Mechanical and Industrial Engineering
University of Toronto
5 King's College Circle
Toronto, Ontario, Canada, M5S 3G8

Corresponding Author:
N. A. Slavinskaya
Institute of Combustion Technology
German Aerospace Centre (DLR)
Pfaffenwaldring 38-40
70569, Stuttgart, Germany
phone: +49 711 6862 543
fax: +49 711 6862 578
nadja.slavinskaya@dlr.de

Abstract:

A chemical kinetic mechanism for C_1 and C_2 fuel combustion and PAH growth, previously validated for laminar premixed combustion, has now been modified and applied to opposed flow diffusion flames. Some modifications and extensions have been made to the reaction scheme to take into account recent kinetic investigations, and to reduce the stiffness of the reaction model. Updates have been made to the cyclopentadienyl reactions, indene formation reactions, and aromatic oxidation and decomposition reactions. Reverse reaction rate parameters have been revised to account for numerical stiffness. Opposed flow diffusion flame simulation data for ethylene and ethane flames with the present mechanism are compared to data computed using two other mechanisms from the literature and to experimental data. Whereas the fuel oxidation chemistry in all three mechanisms are essentially the same, the PAH growth pathways vary considerably. The current mechanism considers a detailed set of PAH growth routes, and includes hydrogen atom migration, possible free radical addition schemes, methyl substitution/acetylene addition pathways, cyclopentadienyl moiety in aromatic ring formation, and numerous reactions between aromatic radicals and molecules. It is shown that while bulk flame properties and major species profiles are the same for the three mechanisms, the enhanced PAH growth routes in the present mechanism are necessary to numerically predict the correct order of magnitude of PAHs that were measured in the experimental studies. In particular, predicting concentrations of naphthalene, phenanthrene, and pyrene, to within the correct order of magnitude with the present mechanism show a significant improvement over predictions obtained using mechanisms in the literature. Sensitivity and production rate analyses show that this improvement is attributable to the enhanced PAH growth pathways and updated reaction rates in the present mechanism. The overreaching goal of this research is to generate and fully validate a detailed chemical kinetic mechanism, with as few fitted rates as possible, that can be applied to premixed or diffusion systems, and used with any type of soot model. To that end, in recently published works, the present mechanism has been used to simulate premixed flames, while coupled to a method of moments to determine soot formation, and to simulate diffusion flames, while coupled to a sectional representation for soot formation. The present work extends the validation of the mechanism by applying it to counterflow diffusion flames, for which measurements of large PAH molecules are uniquely available. The validation of PAH growth predictions are of key interest to soot modelling studies as soot inception from PAH combination and PAH condensation are often major constituents of soot production.

Keywords: counterflow diffusion flame, PAH growth, soot precursor, ethylene, ethane

1. Introduction

The ability to accurately model soot particle nucleation from polycyclic aromatic hydrocarbons (PAHs) remains an important goal of the combustion research community. PAHs and soot particles that are emitted from combustion devices are known to be carcinogenic and contribute to global climate change [1]. A detailed fundamental understanding of PAH growth and soot particle nucleation could aid researchers in developing accurate fundamental models of soot formation. Although much progress has been made, a complete understanding of PAH formation and soot particle nucleation still eludes researchers.

In combustion systems, PAH and soot formation are interdependent through numerous processes. PAHs are known to combine to form incipient soot particles, which then grow and aggregate into large structures. PAHs also contribute to the soot growth process by condensing directly onto the surface of soot particles, and by consuming other smaller chemical species during growth, which would otherwise react with and bind to the soot particles [2,3]. Accurately modelling PAH concentrations within a combustion system is a necessary step to determining soot inception and growth. PAH model development remains a challenging task because there are few experimental data sets suitable for validation, and characterizing the chemistry of PAH growth can involve numerous growth pathways and hundreds of chemical reactions [4].

Frenklach and coworkers have studied the problem of PAH growth and linking PAH and soot formation in premixed flames (see, for example, [5,6,7,8,9]). They demonstrated that mass growth of PAH soot precursors could be modelled primarily using the hydrogen-abstraction-acetylene-addition (HACA) mechanism [7]. They went on to modify their PAH growth mechanism and couple pyrene (A4) concentrations to soot growth in a variety of laminar premixed flames of C_2 hydrocarbons [8]. The PAH growth mechanism used in [8] was based on the chemistry set from [7] but also included C_4H_4 and acenaphthalene (A2R5) reactions. For some systems, Frenklach and coworkers noted significant underprediction in A4 concentrations, suggesting that the PAH growth model was incomplete.

Marinov et al. investigated aromatic and soot precursor formation in rich premixed methane, ethane, ethylene, and propane flames [10], and subsequently augmented the model so it could be applied to a rich, sooting, *n*-butane-oxygen-argon burner stabilized flame [11]. Their PAH growth mechanism considers HACA schemes, as well as several pathways involving odd carbon addition schemes and resonantly stabilized free radicals (propargyl, allyl, 1-methylallenyl, cyclopentadienyl and indenyl). Despite good prediction of the three-ring aromatic molecules, anthracene and phenanthrene (A3), A4 concentrations were underpredicted by more than one order of magnitude in these works as well. The results [10,11] suggest that the addition of the resonantly stabilized free radical pathways has considerably improved PAH growth up to three aromatic rings, but that the set of A4 formation pathways was again incomplete.

Another large body of work by D'Anna, Kent, and coworkers in the last decade has looked at aromatic formation, primarily in ethylene [12] and methane [13] diffusion flames, adding a considerable amount of PAH growth pathways from benzene (A1) to naphthalene (A2) including cyclopentadienyl combination and propargyl addition, in addition to standard HACA. Those first two works were extended to include soot modelling [14,15,16]. Results obtained in [12] agreed well with the experimental data sets for two different ethylene/air flames; one studied first by McEnally and Pfefferle [17] and one by Santoro et al. [18]. However, in isolated regions of the flame, overprediction of acetylene and benzene in [14] and "soot precursors" in [15] was accompanied by an underprediction in soot formation. Therefore, their results also suggest an incomplete model linking gas phase chemistry to soot inception and growth.

Previously, D'Anna and coworkers [19,20] had considered the growth of aromatics up to three rings, including the formation of benzene, phenyl acetylene, indene, biphenyl, naphthalene, acenaphthylene, and phenanthrene. This model had been constructed using only two or three global reactions for each aromatic growth step, the set of which originated from works by Frenklach and coworkers and Marinov and coworkers. This model was tested [12,19,20,21] against ethylene laminar premixed and non-premixed data. However, only bulk aromatic properties, such as total aromatic content were used for PAH submechanism validation.

This model was further extended [22] to describe the growth of aromatics beyond three rings through coagulation processes, referred to by D'Anna and coworkers as "chemical coagulation". Further investigations [14,23,24,25,26] focused on applying sectional method principals to couple the gas phase mechanism to the soot particle phase. These more recent works included integrating the GRI mechanism [27] to model C_1 to C_4 chemistry in [14], increasing the rates of recombination of benzyl with propargyl and of cyclopentadienyl by a factor of 100, and removing indenyl recombination. Despite these studies, D'Anna and coworkers point out [26] that results are still only qualitative and that further development is needed. To address some of these issues, the present work seeks to further and more thoroughly validate a fully detailed and fundamental PAH growth submechanism, for use in soot models. The overreaching goal being to obtain a chemical kinetic mechanism, with as few fitted rates as possible, that can be applied to premixed or diffusion systems, and used with any type of soot model.

It is clear that detailed and accurate PAH growth mechanisms are necessary if accurate simulation of particle inception is to be realized. The collection of studies by Frenklach and coworkers, D'Anna and Kent and coworkers, and the studies by Marinov et al. all point to the difficulty of correctly modelling PAH growth up to large aromatics and subsequent soot particle inception. In addition to those studies, Böhm and coworkers have looked at PAH growth in acetylene and benzene pyrolysis [28,29] and in counterflow diffusion flames burning methane [30]. These works consider methyl, propargyl, cyclopendadienyl, and aryl addition pathways for large PAHs [29] and clearly demonstrate the importance of numerous growth pathways in an opposed flow methane diffusion flame [30]. The present work seeks to build upon this knowledge base of PAH growth in opposed flow diffusion flames by considering additional PAH growth pathways, and applying the mechanism to the C_2 fuels, ethylene and ethane, which have a more complex set of PAH growth routes.

Recently, Slavinskaya and Frank [31] proposed a mechanism for C_1 and C_2 fuel combustion and PAH growth up to five-ring aromatics. Their collection of species and reactions was based on a survey of the literature of the last 30 years and includes comprehensive information about numerous pathways previously considered in the literature. In addition to HACA growth, the mechanism considers hydrogen atom migration, free radical addition schemes, methyl substitution pathways, cyclopentadienyl moiety in aromatic ring formation, and reactions between aromatic radicals and stable aromatic molecules. Thirteen different C_1 to C_6 compounds were used as "building blocks" for PAH molecule growth and for the H atom abstraction from hydrocarbons. In the present work, the mechanism has been modified and extended to opposed flow diffusion flames of ethylene and ethane. Some modifications have been made to the reaction scheme to take into account recent literature, and to reduce the stiffness of the reaction model. Updates have been made to the cyclopentadienyl reactions, indene formation chemistry, and aromatic molecule oxidation and decomposition schemes. Reaction rate parameters were recalculated to account for numerical stiffness that was present in diffusion systems, while the integrity of the mechanism with regard to premixed combustion was carefully maintained.

The present work seeks to further validate the C_2 combustion and PAH growth chemical kinetic mechanism by comparing computations of non-premixed flames of ethylene and ethane in the counterflow geometry to experimental data. Olten and Senkan [32] performed detailed measurements

of major chemical species and aromatics in an opposed flow diffusion flame burning ethylene, and Vincitore and Senkan [33] used the same technique to characterize a similar flame burning ethane. Although there is considerable scatter and uncertainty in the data, the measurements of Senkan and coworkers are very useful for characterizing flame structure, and the orders of magnitude of PAH concentrations. Computations are performed with the present mechanism, and for further comparison, with the mechanisms of Appel et al. [8] and Marinov et al. [11].

In the next section, the three chemical kinetic mechanisms that are used in the present study are outlined and compared. Section 3 presents the flame configuration and numerical model. Computed results obtained with the three mechanisms, comparisons to experimental data, and discussion are found in Section 4. Finally, a summary and conclusions, as well as some future perspectives are highlighted in Section 5.

2. Chemical kinetic model

2.1 Base mechanism development

The chemical reaction mechanism used in the present study describes C_1/C_2 fuel combustion and PAH formation in a semi-detailed manner. The 93 species and 719 reactions describing the growth and oxidation of PAHs in laminar premixed sooting and near-sooting methane and ethylene flames have been presented previously in a detailed manner [31], and have been modified in the present work. The mechanism predicts experimentally determined flame speeds of methane and ethylene reasonably well [31]. Experimental/numerical comparisons in [31] also include concentration profiles of small molecules and radicals, medium-size and high molecular mass aromatic rings, and soot volume fractions measured by 12 different groups in 19 laminar premixed flames. Different C/O ratios, pressures, and shock tube conditions were also considered [31]. A recent study by Dworkin et al. [34] considers the application of an updated version of this mechanism to sooting coflow diffusion flames burning ethylene. It was shown in [34] that soot concentrations in the central region of the flame could be predicted much more accurately than with other mechanisms in the literature. A detailed description of the mechanism and the modifications that have been made to it since it was published in [31] are outlined below. Short forms for chemical names that are used in this article can be found in Table 1.

Table 1. Short forms for chemical names used throughout this article.

Chemical Name	**Short form**
Benzene	A1
Naphthalene	A2
Acenapthalene	A2R5
Biphenyl	P2
Phenanthrene	A3
Pyrene	A4
benzo(ghi)fluoranthen	BGHIF
benzo(a)pyrene	BAPYR

This mechanism [31] is based on the H/O, C_1, and C_2 chemistry of the Leeds methane oxidation reaction scheme presented in [35] and includes its later updates [36] with regard to the H_2/CO submechanism. The thermochemical data used in [35] and [36] is based on the experimental

measurements and recommendations of Baulch et al. [37] and Burcat [38]. This set of reactions has been selected as the base chemistry model for the development of the DLR reaction database with an aim to reduce both the amount of optimized or fitted rate constants, and the need for subsequent refitting and reoptimization of the small chemistry data, as much as possible.

The presented kinetic scheme is the basis for reaction mechanisms of larger hydrocarbons (up to $C_{16}H_{34}$) that are used for combustion simulations of various high-molecular weight fuels [39]. The overall reaction model has a strong hierarchical structure and is developed to be applicable to combustion modelling of practical fuels in a wide range of operating conditions relevant to gas turbines. Recently, a surge in interest in syngas combustion has provoked active investigation of $CO/H_2/O_2$ chemistry and has resulted in new thermokinetic data. As the H_2/CO kinetics play a primary role in the fundamental hierarchal structure of hydrocarbon combustion chemistry, this submechanism has been reviewed and upgraded. Newly published thermochemical data [37,40,41,42,43] has been incorporated into the mechanism. As was noted in [31], the reactions of H_2/O_2 strongly influence the formation of PAH precursors, and therefore, their kinetics are revisited and adjusted here. Modifications to the hydrogen submechanism are described below.

The following new reactions have been added to the model:

$$HO_2 + HO_2 = H_2O_2 + O_2 \quad (1)$$
$$O + OH + M = HO_2 + M \quad (2)$$
$$H_2 + O_2 = OH + OH \quad (3)$$

with rate coefficients taken from [37], [40], and [41], respectively.

For the set of reactions,

$$2H + Ar/N_2/H_2/H_2O/H = H_2 + Ar/N_2/H_2/H_2O/H \quad (4)$$
$$OH + H_2 = H_2O + H \quad (5)$$
$$H + O_2 (+ M/Ar/O_2/H_2O) = HO_2 (+ M/Ar/O_2/H_2O) \quad (6)$$
$$H + HO_2 = H_2 + O_2 \quad (7)$$
$$H + HO_2 = 2OH \quad (8)$$

rate coefficients have been updated. For reaction (4), a value based on the recommendation in [42] has been applied. For reaction (5), rate coefficients obtained from *ab initio* data presented in [43] have been adopted. A review of data in the literature for reaction (6) resulted in the replacement of rate coefficients used in the Leeds mechanism [35,36] with recommendations provided in [44]. Values of reaction rates for (7) and (8) from [37] have been modified within the range of their stated uncertainty: increased and decreased, respectively, by a factor of 0.3. These modifications primarily improve the oxidation chemistry. This improvement is demonstrated by the comparisons of ethylene ignition delay simulations with measurements [45,46,47,48] obtained for different mixtures and dilutions. Simulations and comparisons to these experimental data are presented in Fig.1 a-d (in which "pw" denotes the "present work") for pressures from 1 to 3 atm and in Fig. 2 for recently published high-pressure data [49]. Results of simulations of laminar flame speed are similar to those presented in [31]. Testing and verifying the ignition kinetics of a chemical kinetic mechanism is a good test to ensure that the mass flux of small radicals, which also play an important role in PAH formation, can be correctly reproduced.

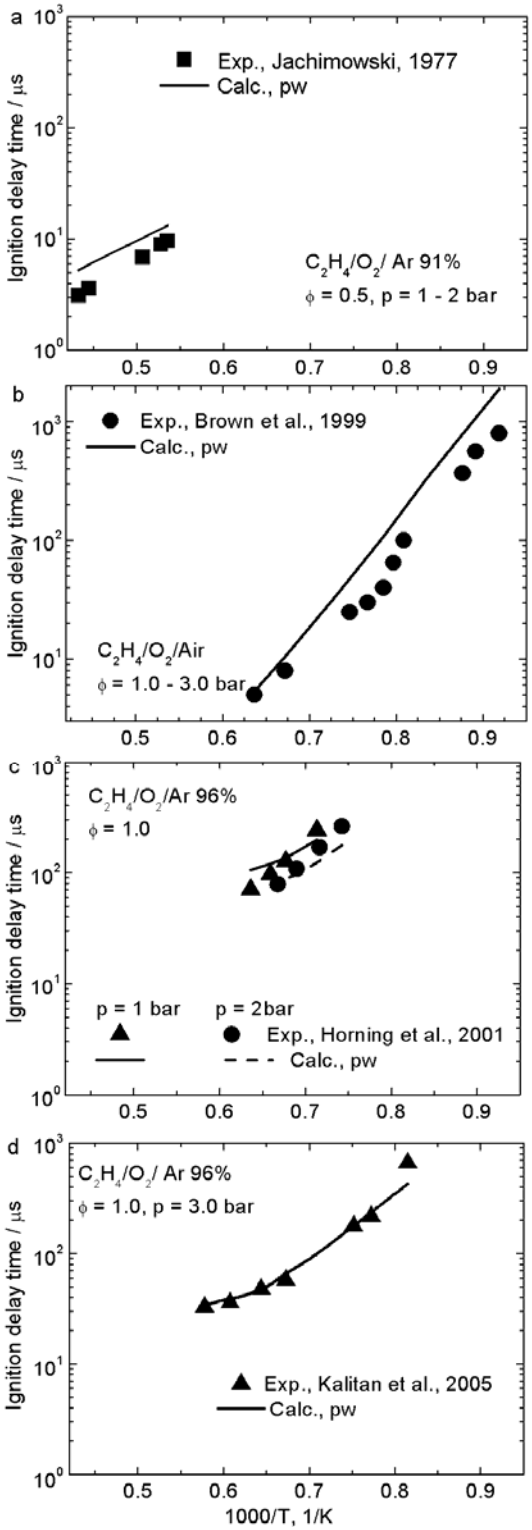

Fig. 1. Comparison of simulated ignition delay time for ethylene with experimental data for the datasets of a) Jachimowski [45], b) Brown and Thomas [46], c) Horning [47], and d) Kalitan et al. [48].

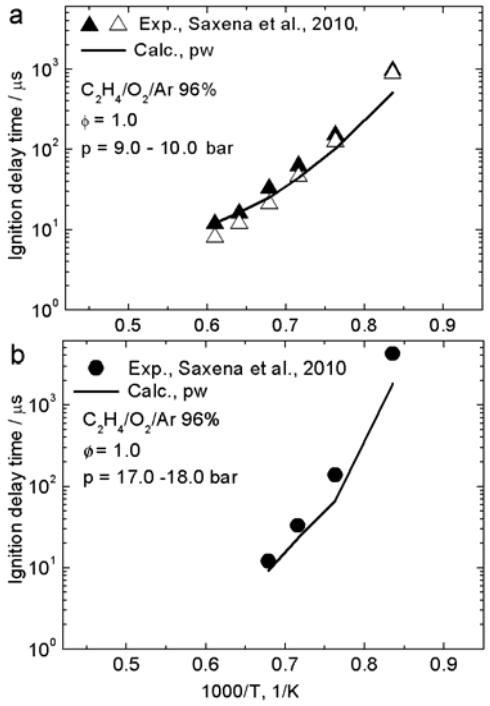

Fig. 2. Comparison of simulated ignition delay time for ethylene with experimental data from Saxena et al. [49] for pressures of a) 9 – 10 bar, and b) 17 – 18 bar.

2.2 PAH growth mechanism development

Further review of the literature and testing has been performed in order to update the chemical kinetic and thermodynamic data of the PAH growth submechanism. The thermokinetic data for cyclopentane, benzyl, and indene, which are all key species involved in PAH formation, have been updated to reflect the current state of the literature. Reaction pathways involving cyclopentadienyl radical were revised based upon a series of investigations [50,51,52,53]. In Zhong and Bozzelli [50], a submechanism of important cyclopentadienyl radical reactions has been assembled and tested in an elementary model for benzene combustion. Here, the reaction for A1 formation,

$$C_5H_6 + C_2H_3 = A1 + CH_3 \qquad (9)$$

has been introduced in the model with the rate coefficient $k = 2.12 \cdot 10^{67} T^{-16.08} \exp(-21320/T)$, with units of *mol, s, K,* and *cm* (and henceforth). This coefficient has been evaluated from literature data and from group additivity rules with hydrogen bond increments.

Benzene formation as the subsequent stage to methyl and cyclopentadienyl radical combination to form fulvene has been investigated in [51]. The two-reaction sequence of $CH_3 + C_5H_5 \rightarrow C_5H_5CH_3$ and $C_5H_4CH_3 \rightarrow$ fulvene + H was proposed. Taking in consideration the reaction rate of fulvene isomerisation to benzene [52] this sequence has been adopted as the global path,

$$C_5H_5 + CH_3 = A1 + 2H \qquad (10)$$

with a rate coefficient evaluated of $k = 1.00 \cdot 10^{18} \exp(-30000/T)$.

Lindstedt et al. [51] also speculatively proposed that phenylacetylene may be formed via analogous reactions of propargyl with cyclopentadienyl,

$C_5H_5 + H_2CCCH \rightarrow C_8H_7(F) + H$ (11)
$C_8H_7(F) \rightarrow A1C_2H + H$ (12)

The proposed channel has been introduced in the mechanism as a single step reaction,

$C_5H_5 + H_2CCCH = A1C_2H + 2H$ (13)

with a reaction rate of $k = 3.00 \cdot 10^{16} \exp(-29131/T)$, which also accounts for phenylacetylene formation via n-C_8H_7.

Kinetics data, calculated and measured for one of the most important cyclopentadienyl formation reactions,

$H_2CCCH + C_2H_2 = C_5H_5$ (14)

have been determined in time-resolved experiments as a function of temperature (800-1100 K) using the Laser Photolysis/Photoionization, technique [53]. Accordingly, a resultant reaction rate constant of $k = 2.40 \cdot 10^{11} \exp(-5030/T)$, is used in the present mechanism.

In [53], C_5H_5 was detected as a primary product of reaction (14). Formation of C_7H_7 was observed with kinetics corresponding to that of a secondary reaction and further formation of indene. These experimental results are in qualitative and quantitative agreement with the investigation of Kislov and Mebel [54], in which the *ab initio* G3(MP2,CC)//B3LYP calculations of the potential energy surface for the formation of indene involving benzene, benzyl, phenyl, propargyl, and methyl radicals, and acetylene, have been performed. Kislov and Mebel [54] investigated the build-up of an additional cyclopenta moiety over the existing six-member aromatic ring. The study was augmented by statistical calculations of high-pressure limit thermal rate constants in the temperature range of 300-3000 K for all reaction steps utilizing conventional Rice-Ramsperger-Kassel-Marcus and transition-state theories. The rate obtained for the overall sequence, $C_7H_7 + C_2H_2 \rightarrow$ INDENE + H is similar to the rate of reaction (14) measured in [53]. Accordingly, coefficients for reactions,

$C_7H_7 + C_2H_2 \rightarrow$ INDENE + H (15)
$C_5H_5 + C_4H_4 =$ INDENE + H (16)
$C_5H_5 + C_4H_2 =$ INDENYL (17)

were updated to reflect the values proposed in [53].

Considering the potential importance of the propargyl radical suggested in [54], its reactions with A1 and phenyl are anticipated to be significant sources of indene. In the case of A1, one must consider a molecular-radical mechanism, that is, intermolecular addition of propargyl to the π-system of A1, whereas with phenyl, the reaction sequence is initiated by the association of phenyl and propargyl radicals, followed by radical activation of a recombination product.

The reaction of propargyl radical with A1 proceeds through several rearrangements on the C_9H_9 potential energy surface, which follow an initial addition step. In this case, the sequence: A1 $\rightarrow$ B1 $\rightarrow$ B2 $\rightarrow$ C3 $\rightarrow$ T5 $\rightarrow$ indene + H can be considered as the favoured path to indene. Here, the nomenclature from [54] is used: B1 is a benzyl isomer; and B2, C3 and T5 are isomers of C_9H_9. This channel was introduced in the mechanism with the rate limiting step in the sequence,

A1 + H2CCCH → INDENE + H, (18)

and a reaction rate of $k = 1.50 \cdot 10^{14} \exp(-25912.2/T)$ [54]. This reaction rate is also used in the analogous reactions,

INDENE + H_2CCCH → A2R5 + H + H_2. (19)

and

INDENE + H_2CCCH → P2 + H. (20)

The A1- + H_2CCCH recombination mechanism requires fewer reaction steps to form indene, and exhibits lower energy barriers (14-17 kcal/mol), as compared to the pathway beginning with propargyl addition to benzene. Two channels of indene formation from phenyl with similar energetics have been identified and are presented in [54]. The limiting step in the sequence A1- + H_2CCCH → B10/B11 → B12/B14 → B13 → indene (B10, B11, B12, B13 and B14 are isomers of C_9H_9 [54]) was utilized for the rate coefficient for the global reaction,

A1- + H_2CCCH → INDENE, (21)

with a reaction rate of $k = 3.86 \cdot 10^{12} \exp(-6850.5/T)$ [54]. This rate has also been adopted for the analogous reactions,

C_7H_7 + H_2CCCH → A2 + 2H, (22)
INDENYL + H_2CCCH → P2 (23)

and

A2CH_2 + H_2CCCH → A3 + 2H. (24)

The thermal decomposition reactions of the benzyl radical,

$C_7H_7 = C_4H_4 + H_2CCCH$ (25)
$C_7H_7 = C_5H_5 + C_2H_2$ (26)

were revised taking into account experimental data obtained in [55]. Measurements were performed for reflected shock waves with temperatures ranging from 1430 to 1730 K at total pressures around 1.5 bar. Rate parameters for these reactions have been optimised for the experimental data in [55] and for results of premixed laminar flame simulations. For reactions (25) and (26), the rate constants are determined as $k = 2.00 \cdot 10^{14} \exp(-42300.0/T)$ and $k = 6.00 \cdot 10^{13} \exp(-35000.0/T)$, respectively. In addition, based on the data in [55], the preexponent of the Arrenius form for the rate coefficient for A1 = C_4H_4 + C_2H_2 from [37] has been decreased by a factor of 10.

The possible reaction paths to indene have been investigated in a quantum chemistry study devoted to the formation of PAH and soot precursors through butadiene reactions [56]. Kinetic constants for each elementary reaction involved in the reactive processes were calculated at the B3LYP/6-31g(d,p) level with conventional transition state theory, while overall rate constants for the formation of the different products were determined with Quantum Rice-Ramsperger-Kassel theory.

Reactions pathways to indene involving butadiene have been incorporated in the mechanism via the global reaction,

C_4H_6 + A1- = INDENE + CH_3, (27)

with a reaction rate $k = 1.42 \cdot 10^{13} \exp(-14000/T)$. This rate has also been adopted for an analogous reaction with similar energetics,

i-C_4H_5 + A1 = INDENE + CH_3. (28)

Adjustments have also been made to the mechanism for reactions of 2- , 3-, and 4- aromatic ring molecules with O and OH radicals. These modifications have been implemented based on the investigation of Mati et al. [57], wherein the kinetics of oxidation of 1-methylnaphthalene have been studied in a jet stirred reactor (T = 800 - 1421 K, p = 1 - 10 atm, equivalence ratio = 0.5 - 1.5). Molecular species concentration profiles of reactants, stable intermediates and final products were measured by sonic probe sampling followed by on-line GC-MS analyses and off-line GC-TCD-FID and GC-MS analyses. Based on these results, the reaction rate of

A2 + O = A2- + OH (29)

has been changed to $k = 2.00 \cdot 10^{14} \exp(-7400.0/T)$. The same rate coefficient has been prescribed to the following reactions of A2R5 and benzo(ghi)fluoranthen with an oxygen radical, which exhibit similar energetics:

A2R5 + O → A2- + HCCO (30)
BGHIF +O = HCCO + A4- (31)

For ring-opening reactions of heavy aromatics with O and OH radicals, which are endothermic by approximately 40 kcal/mol relative to the reactants, the activation energy has been increased with respect to the value proposed by Wang and Frenklach [7]. Several reactions have been prescribed as irreversible in order to reduce the numerical stiffness of the system, which was caused by unrealistic rates for reverse reactions calculated from equilibrium constants at temperatures below 1000 K. For this reason, dissociation reactions of A4, benzo(ghi)fluoranthen and benzo(a)pyrene have been replaced with the irreversible recombination reactions:

C_4H_2 + A2R5 → A4 (32)
A2R5 + $C6H_2$ → BGHIF (33)
A2 + C_8H_2 → BGHIF (34)
C_4H_2 + A4 → BAPYR (35)

Rate coefficients for (32) – (35) have been determined by analogy to the reverse rate of the reaction A1 = C_4H_4 + C_2H_2 from [37]. The numerical tests performed (which calculated species concentration profiles and equilibrium distributions of concentrations) demonstrate that the model is not sensitive to the irreversibility introduced for some decomposition reactions.

The modifications described herein have improved the model predictions of PAH concentrations, both qualitatively and quantitatively and in some cases have reduced the disagreement by an order of magnitude to a factor of two to three (for the worst cases published in [31]). To avoid repeating the figures of [31], only simulation data of PAHs and their precursors in the laminar ethylene

premixed flame of Castaldi et al. [58] are presented here. These images are intended to illustrate the validation and improvements of the revised model.

Comparisons for the small molecules, C_2H_2, C_4H_2, C_4H_4, and C_4H_6, (see Fig. 3), show excellent agreement between the new computational data and the experiments of Castaldi et al. [58]. In particular, the computed data for C_4H_6 demonstrates considerable improvement when compared to [31]. Comparisons for one-ring aromatics are shown in Fig. 4. Other than a slight improvement in the predicted benzene concentrations at x > 0.6 cm, the data are similar to that of [31], again showing very good agreement.

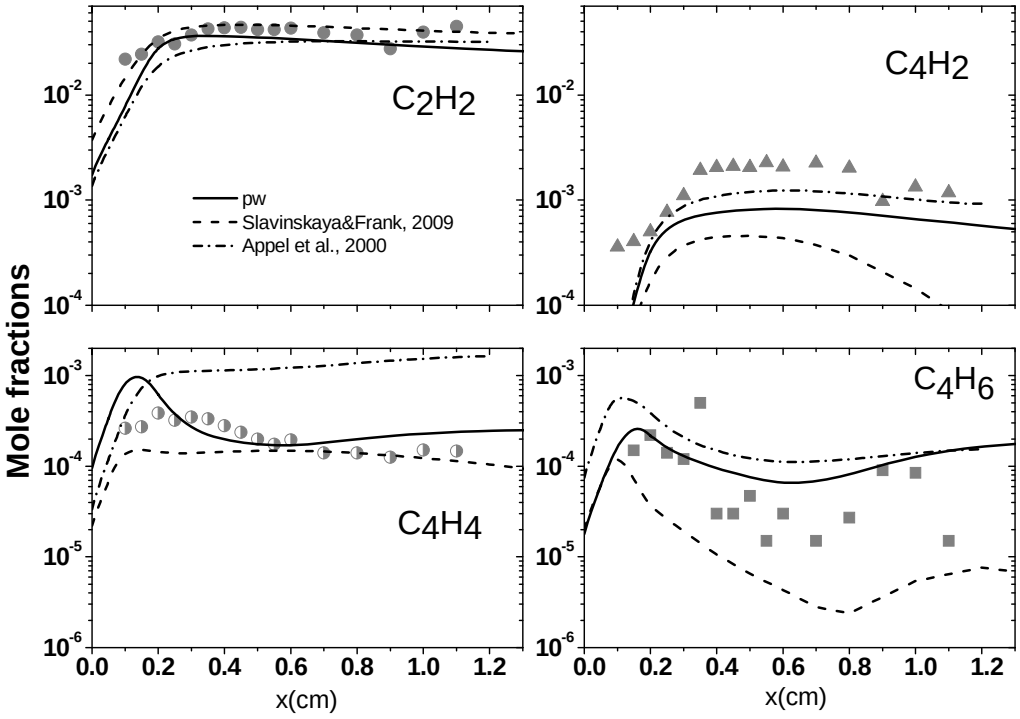

Fig. 3. Small molecules in the premixed laminar $C_2H_4/O_2/Ar$ flame studied experimentally in [58]. Pressure p = 1 bar, ϕ = 3.06. Symbols – experimental data from [58], lines – calculations.

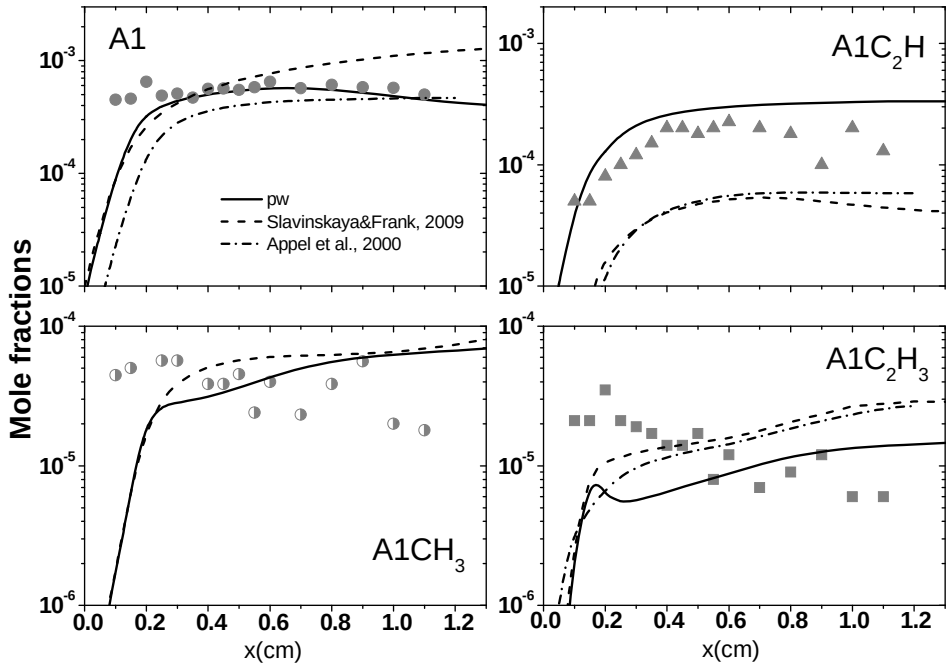

Fig. 4. One-ring aromatic molecules in the premixed laminar C_2H_4/O_2/Ar flame studied experimentally in [58]. Pressure p = 1 bar, ϕ = 3.06. Symbols – experimental data from [58], lines – calculations.

Comparisons for naphthalene and the five-member ring aromatics are also quite promising. Very good agreement is shown for these species in Fig. 5, in which it can be seen that the underpredictions of indene, naphthalene and acenaphthalene that were present in [31], have been reduced or eliminated. Finally, comparisons for the larger aromatics are plotted in Fig. 6, in which the excellent agreement that was present in [31] has been maintained.

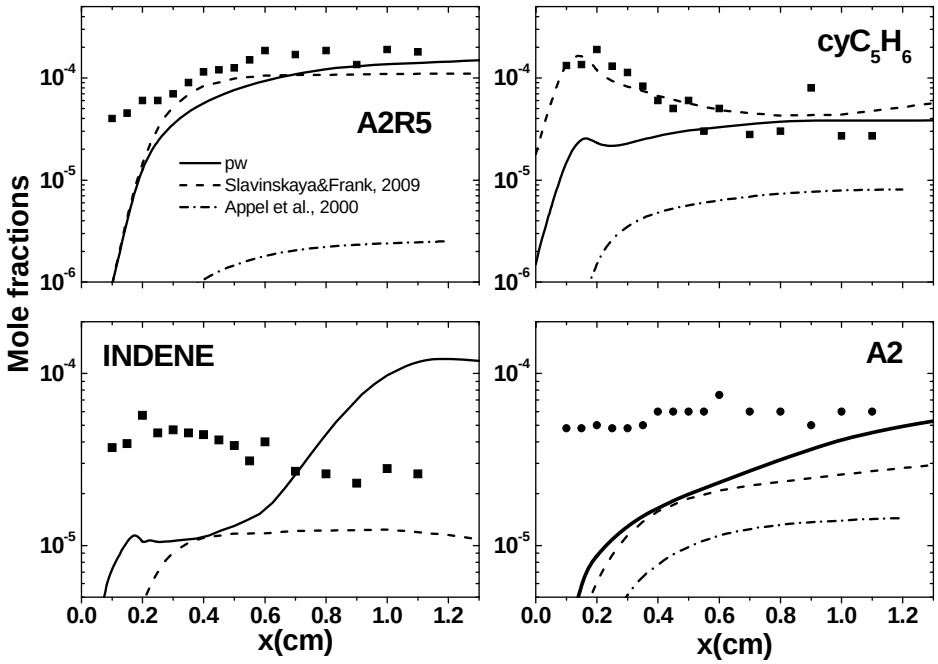

Fig. 5. Naphthalene and molecules with a five-member ring in the premixed laminar C_2H_4/O_2/Ar flame studied experimentally in [58]. Pressure p = 1 bar, ϕ = 3.06. Symbols – experimental data from [58], lines – calculations.

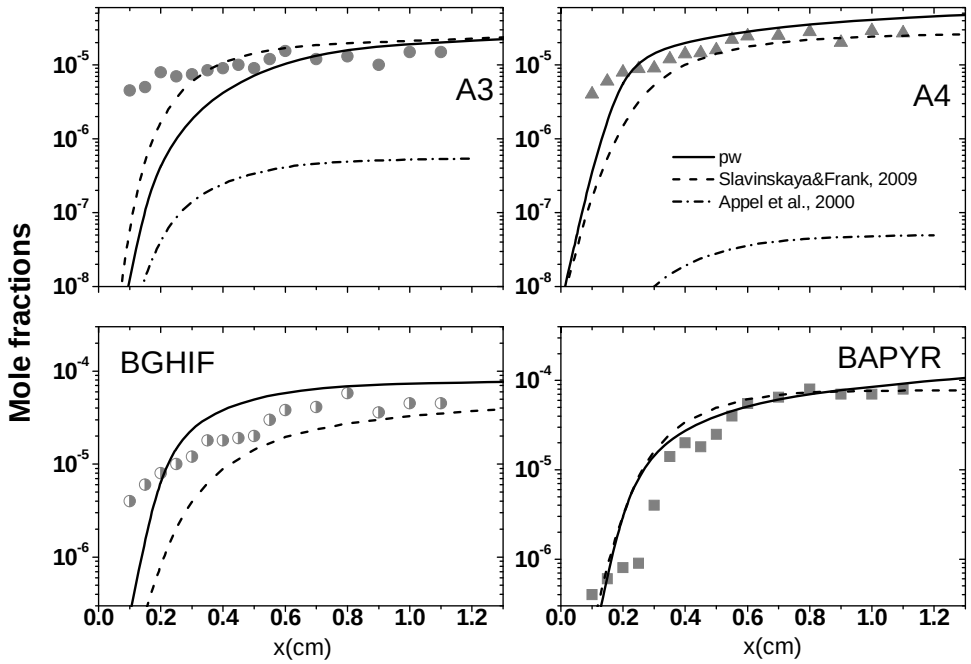

Fig. 6. Three-, four-, and five-ring aromatic molecules in the premixed laminar C_2H_4/O_2/Ar flame studied experimentally in [58]. Pressure p = 1 bar, ϕ = 3.06. Symbols – experimental data from [58], lines – calculations.

3. Flame and model description

The present work aims to simulate two different counterflow non-premixed flames; an ethylene flame that has been studied experimentally by Olten and Senkan [32], and an ethane flame that was the

subject of a similar study by Vincitore and Senkan [33]. For each flame, a mixture of either ethylene or ethane with argon flows from a cylindrical fuel port, against a mixture of oxygen and argon flowing from an opposing cylindrical port. The flow configuration is shown in Fig. 7. Counterflow diffusion flames were chosen in part due to their non-premixed nature (the present mechanism was already validated for premixed combustion), and because the experimental studies include detailed PAH measurements, which are essential for validating the PAH growth reaction schemes.

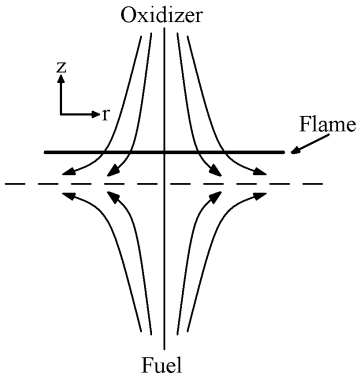

Fig. 7. Schematic representation of a counterflow diffusion flame

The ethylene flame, known hereafter as flame1, is at atmospheric pressure, sooting, flat, and laminar. The fuel and oxidizer ports are separated by a distance of 1.5 cm and the resulting flame has a strain rate of 37.7 s^{-1}. The flow conditions and burner properties, reproduced from [32], are shown in Table 2. These flow conditions generate a stable flame, with a yellow luminous zone, indicative of soot formation between 0.4 cm and 0.8 cm from the fuel port [32]. Soot formation and particle dynamics are not included in the model. This is an acceptable assumption since low soot concentrations are expected in this flame.

Table 2. Flow conditions and burner properties for flame1.

Property	Fuel Port	Oxidizer Port
Velocity	13.16 cm/s	16.12 cm/s
Argon mole fraction	0.25	0.78
C_2H_4 mole fraction	0.75	0.0
O_2 mole fraction	0.0	0.22
Density	1.27×10^{-3} g/cm^3	1.56×10^{-3} g/cm^3
Temperature	298	298
Port diameter	2.54 cm	2.54 cm

The ethane flame, which will be known as flame2, employs a similar setup to flame1. Other than burning ethane, the port separation distance is slightly increased to 1.63 cm, the strain rate is slightly reduced to 35.0 s^{-1}, and the oxidizer concentration has been increased slightly. The flow conditions and burner properties for flame2, reproduced from [33], are shown in Table 3. Flame2 also has a yellow luminous zone indicative of soot formation that is visible between 0.2 cm and 0.6 cm from the fuel port [33].

Table 3. Flow conditions and burner properties for flame2.

Property	Fuel Port	Oxidizer Port
Velocity	13.16 cm/s	16.12 cm/s
Argon mole fraction	0.25	0.8
C_2H_6 mole fraction	0.75	0.0
O_2 mole fraction	0.0	0.2
Density	1.33×10^{-3} g/cm^3	1.57×10^{-3} g/cm^3
Temperature	298	298
Port diameter	2.54 cm	2.54 cm

The kinetic modeling of flame1 and flame2 was performed using the OPPDIF code of the CHEMKIN modeling package [59]. Chemical kinetic, thermodynamic, and transport databases are used as inputs in the CHEMKIN package. Each of the two flames is computed three times; once with the chemical kinetic mechanism of Appel et al. [8], once with the mechanism of Marinov et al. [11], and once with the present mechanism. The computed results, and comparisons to experimental data, are discussed in the following section.

4. Results and discussion

4.1 Results - major species

Computations are performed for flame1 and flame2 using the OPPDIF module of CHEMKIN. For each case, an absolute tolerance of 10^{-9} is used and the grid is adaptively refined until the solution gradient and curvature do not exceed 0.4 [59]. Pseudo timestepping is used to aid convergence from an arbitrary starting estimate. For these conditions and tolerances, the algorithm will successively add up to about 70 to 80 grid points. Care was taken to ensure grid independence of the solutions by lowering the gradient and curvature tolerances to 0.1 and making sure that the solution did not change. The computed data presented here are for a mixture-averaged, "Fickian" type diffusion model. A check was performed to see if the solution would be sensitive to the inclusion of either thermal diffusion, or multicomponent species diffusion and the results indicated negligible changes in the solution profiles.

Computed major species profiles, including CO_2, CO, H_2O, C_2H_4, C_2H_2, and O_2 for flame1 (ethylene) are shown in Fig. 8. Only the computational results generated using the present chemical kinetic mechanism, adapted from [31] are shown, since the major species profiles for all three mechanisms were coincident. In addition, temperature is not shown since it too lay coincident for all three mechanism and corrected thermocouple measurement were not included in the experimental works. It can be seen from Fig. 8a that the profiles of the main combustion products, CO_2, CO, and H_2O are all well-reproduced by the model in terms of the general structure of the diffusion flame. The concentration of CO peaks at 0.63 cm from the fuel port. The location and magnitude of the profile are in good agreement with the experimentally measured values. The other main combustion products, CO_2 and H_2O, peak at 0.8 cm from the fuel port. Both CO_2 and H_2O are underpredicted by the model, however, there are uncertainties in the experiments as detailed in [32], and considerable scatter in the measured data, as is evident in Fig. 8. Therefore these comparisons should be taken as a comparison of general flame structure. More detailed comparisons for major species and temperature can be found in [31,34].

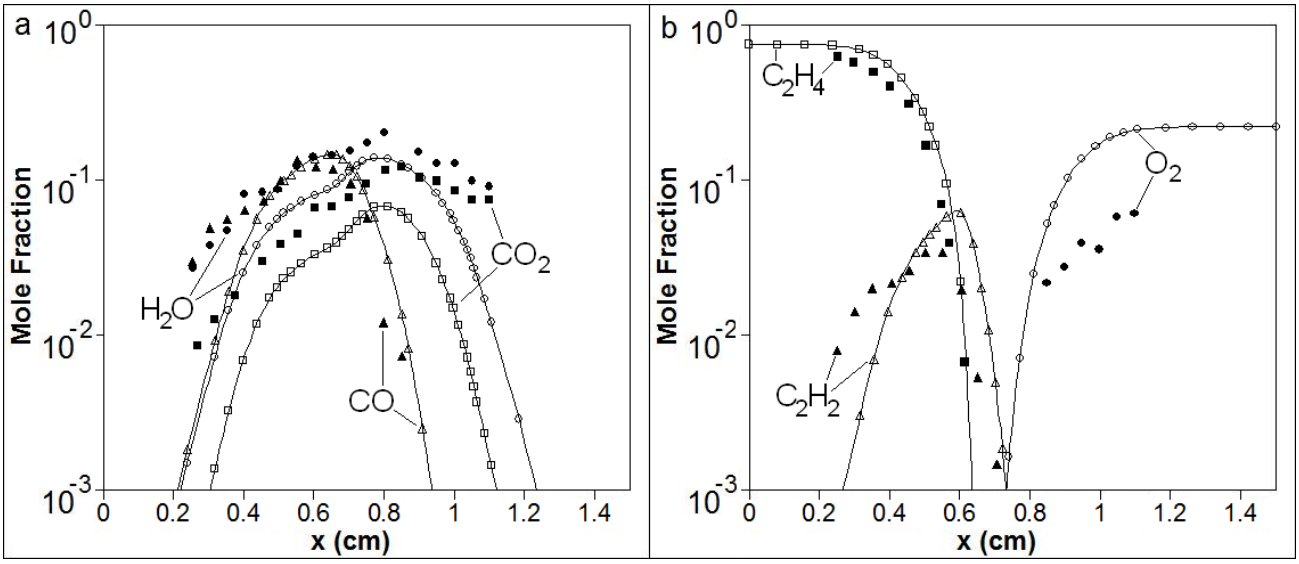

Fig. 8. Comparison of numerical and experimental mole fractions of major species in the counterflow ethylene/air diffusion flame (flame1). Solid symbols are experimental data from [32] and open symbols with curves are numerical values computed with the present chemical kinetic mechanism (modified [31]). a) CO_2 (squares), CO (triangles), and H_2O (circles). b) C_2H_4 (squares), C_2H_2 (triangles), and O_2 (circles).

Fig. 8b shows the experimental and numerical comparison of C_2H_4, C_2H_2, and O_2 profiles. The consumption of C_2H_4 and production of C_2H_2 are consistent between the measurements and the model. In both the measured and computed data, the fuel is completely consumed at 0.63 cm from the fuel port. This distance also corresponds to the location where the concentration of CO peaks, indicating that the model can accurately predict the general properties of fuel consumption and combustion product formation. The model predicts higher concentrations of O_2 near the oxidizer port than the measured data would suggest. The computed data asymptotes to the correct imposed boundary condition value, whereas the trend in the experimental data does not. Since there is considerable scatter in the measured values, and no experimental data within 0.35 cm of the oxidizer port, it is difficult to determine the reason for this discrepancy.

Computed major species profiles for flame2, the ethane/air flame, are shown in Fig. 9. In Fig. 9a, the shape and magnitude of the measured concentrations of CO_2, CO, and H_2O are very well matched by computed profiles, but their locations are offset. The computed profiles are all about 0.25 cm further away from the fuel port than the measured values. An understanding of this offset between the data (the presence of which was independent of the choice of the three chemical kinetic mechanisms) can be partly obtained from Fig. 9b, which shows the computed and experimental mole fractions of C_2H_6, C_2H_2, and O_2. The decomposition of the fuel, C_2H_6, is happening much slower in the model than the experimental data indicates. The offset between the experimental data and numerical predictions for C_2H_6 is also about 0.25 cm, the same offset that is observable for the major species in Fig. 9a, and for C_2H_2 in Fig. 9b. We conclude that there is a need to revisit and refine the treatment of oxidation reaction rates of C_2H_6 in the chemical mechanism, and to more carefully consider the boundary conditions in the experiments, which are commonly known source of uncertainty.

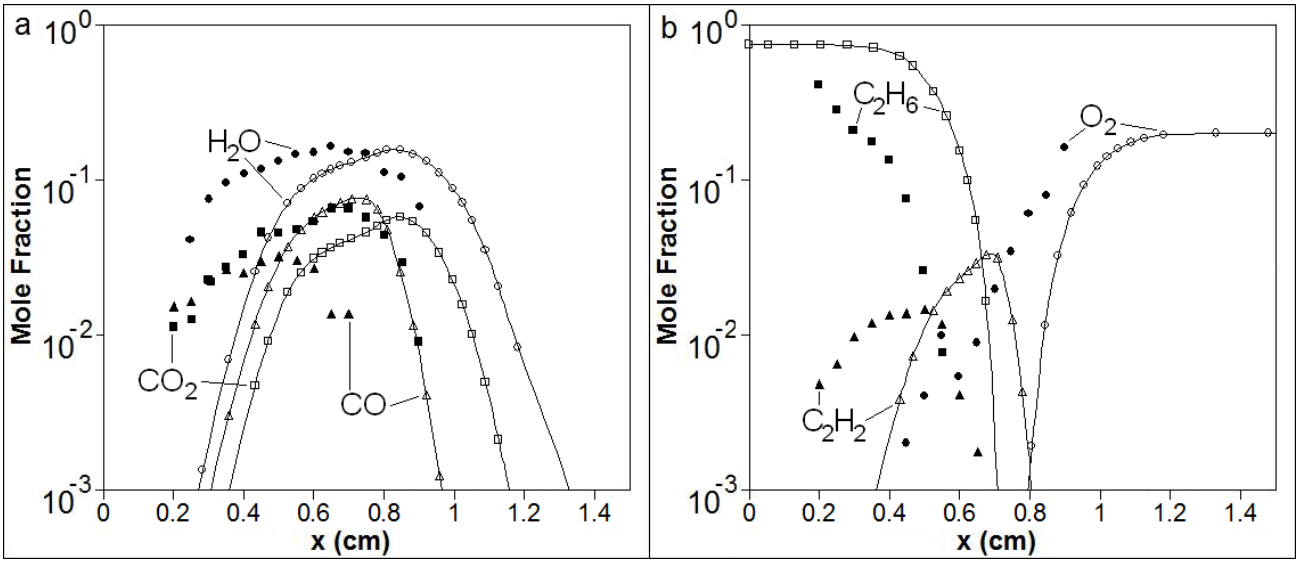

Fig. 9. Comparison of numerical and experimental mole fractions of major species in the counterflow ethane/air diffusion flame (flame2). Solid symbols are experimental data from [33] and open symbols with curves are numerical values computed with the present chemical kinetic mechanism (modified [31]). a) CO_2 (squares), CO (triangles), and H_2O (circles). b) C_2H_4 (squares), C_2H_2 (triangles), and O_2 (circles).

There is also an offset between the computed and measured O_2 profiles in Fig. 9b. Here, the size of the offset is similar to those of the other species (close to 0.25 cm in the flame zone). Other than the shift in these profiles, the computed data reproduces the overall shape and magnitude of the measured data quite well, indicating that the model is capable of reproducing most of the general diffusion flame structure. In light of the overreaching purpose of the present study – to contrast the three chemical kinetic mechanisms by comparing their predictions for PAH concentrations to experimental data – the data sets remain highly relevant. As will be shown in the next section, although there is some scatter and sources of error in the experimental data, and a possible inadequacy in the rates of the primary decomposition reactions of C_2H_6 (which appears consistently in all three of the mechanisms), comparisons of PAH concentrations clearly demonstrate the importance of newly added PAH growth pathways in the present mechanism.

4.2 Aromatics

In addition to validating the present chemical kinetic mechanism using major species profiles obtained for diffusion flames, an objective of the present work is to study aromatic formation and growth components in the mechanism. It is well known that soot formation is controlled by kinetic processes, which take place in the main reaction zone of the flame. These processes mainly comprise a competition between fuel oxidation and the formation of soot precursors, which are strongly influenced by temperature, pressure and C/O ratio. To describe the formation of small and large soot precursors in diffusion flames with the relatively wide parameter distribution present in the main reaction zone, the chemical kinetic reaction model should consider a wide spectrum of channels of the formation of PAHs. Therefore, it is important to investigate how realistically the most up-to-date chemical kinetic models can reflect the PAH chemistry of diffusion flames, and where their current downfalls and areas of further needed investigation may remain.

In the present work, aromatic profiles predicted with the improved version of the recently published mechanism [31] are compared with those predicted by two other chemical kinetic mechanisms that are prominent in the literature (Appel et al. [8] and Marinov et al. [11]), and with the experimental data of Senkan and coworkers [32,33]. The objective here is to see how the additional

PAH growth pathways in the present mechanism augment or enhance aromatic profile predictions as compared to the mechanisms from the literature.

Aromatic and substituted aromatic profiles are compared for flame1 (ethylene) in Fig. 10. In these figures, a logarithmic concentration scale is used so that predictions from the various chemical kinetic mechanisms, which vary by orders of magnitude, can be compared on the same plot. The A1 profile computed with the present mechanism (denoted "pw") is shifted toward the fuel port and exhibits higher peak concentrations than the profiles computed with the other two mechanisms. The peak concentration computed with the other two mechanisms is closer to that of the data measured by Olten and Senkan [32], indicating comparatively weaker performance of the present mechanism in predicting formation of the first aromatic ring. The main reason for this disparity is that the present mechanism incorporates all possible isomers of C_6H_6 under the name of A1. It is worth noting, however, that the shift of the profile toward the fuel port (and toward the experimentally measured profile) marks a slight improvement over the other two mechanisms, which both predict the profile location to be closer to the oxidizer port.

Corresponding and similar results are observed for $A1C_2H$ and $A1C_2H_3$. Here, the overprediction of these two species is a direct result of the overprediction of A1 as they are formed directly from C_1 or C_2 addition to phenyl, which is tied to A1 concentration via various hydrogen abstraction reactions. Despite this reasoning, there still remains a need for the oxidation channels of $A1C_2H$ and $A1C_2H_3$ to be revised. $A1CH_3$ is also compared to experimental data in Fig. 10, but only with the present mechanism and that of Marinov et al. [11] as it is not included in the Appel et al. [8] mechanism. The present mechanism overpredicts the concentration of $A1CH_3$ by nearly an order of magnitude, and the Marinov et al. [11] mechanism underpredicts its concentration by about the same range. It is believed that $A1CH_3$ will play an important role in aromatic growth in methane flames, or systems with appreciable methyl and/or propargyl radical concentrations since small-molecule PAH growth in these systems will not be dominated by C_2 addition. Therefore, $A1CH_3$ chemistry (primarily involving the oxidation of toluene) should remain an area of further study in the development of mechanisms that will be applicable to a wider variety of systems.

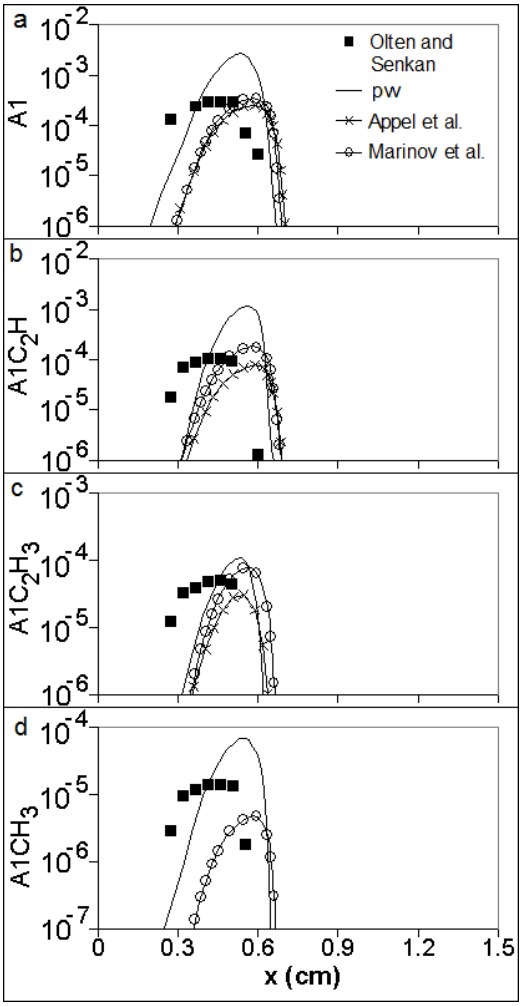

Fig. 10. Comparisons of experimental (from [32]) and numerical profiles of aromatics and substituted aromatics for the first aromatic ring for the C_2H_4/air diffusion flame (flame1); a) benzene (A1) computed with all three chemical kinetic mechanisms, b) $A1C_2H$ computed with all three chemical kinetic mechanisms, c) $A1C_2H_3$ computed with all three chemical kinetic mechanisms, and d) $A1CH_3$ computed with the present mechanism and the mechanism of Marinov et al. [11] only ($A1CH_3$ is not included in the mechanism of Appel et al. [8]).

Aromatic and substituted aromatic profiles for the first aromatic ring are also included for flame2 (ethane) in Fig. 11. As with the major species profiles in Section 4.1, the computed profiles are all considerably closer to the oxidizer port than the experimental data. The reason for this is not yet known and will remain an area of further investigation and potential mechanism improvement. There also seems to be considerable experimental uncertainty with the flame2 dataset (there is more physically unrealistic scatter and non-monotonic concentration fluctuations in the dataset presented in Vincitore and Senkan [33] than that in Olten and Senkan [32]). The concentrations can nonetheless be compared and contrasted and the experimental data are still included for the purposes of knowing approximate values and order of magnitude. For A1, the present mechanism and mechanism of Marinov et al. [11] both overpredict A1 concentrations by about an order of magnitude, whereas the Appel et al. [8] mechanism predicts concentrations that are in line with the experimental data. Not surprisingly, the same trends can be observed for $A1C_2H$ and $A1C_2H_3$. The $A1CH_3$ concentrations are predicted quite well by the present mechanism and overpredicted by the Marinov et al. [11]

mechanism, which suggests that further investigation into $A1CH_3$ is in order since a strong dichotomy exists between the quality of the predictions of the present mechanism for flame1 and flame2.

Despite having known deficiencies and oversimplifications in aromatic growth, the Appel et al. [8] mechanism does a good job predicting concentration levels of A1 and the A1-substituted aromatics. Accurate prediction of A1 and its substituted aromatics are important to modelling growth of multi-ring aromatics and therefore more investigation into its chemistry is needed for the present mechanism.

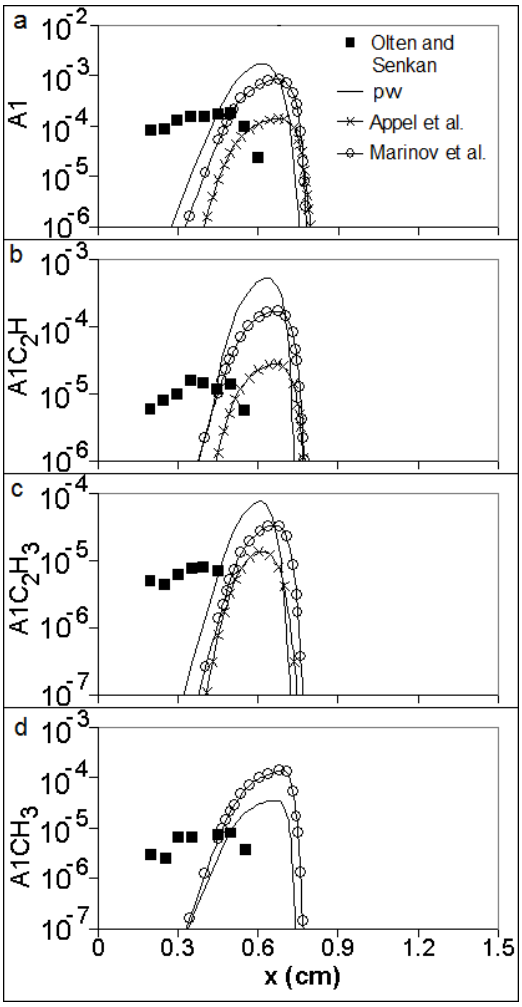

Fig. 11. Comparison of experimental (from [33]) and numerical profiles of aromatics and substituted aromatics for the first aromatic ring for the C_2H_6/air diffusion flame (flame2); a) benzene (A1) computed with all three chemical kinetic mechanisms, b) $A1C_2H$ computed with all three chemical kinetic mechanisms, c) $A1C_2H_3$ computed with all three chemical kinetic mechanisms, and d) $A1CH_3$ computed with the present mechanism and the mechanism of Marinov et al. [11] only ($A1CH_3$ is not included in the mechanism of Appel et al. [8]).

Two-ring aromatic species (A2, A2R5, P2, and indene) are compared with the three mechanisms and experimental data in Fig. 12 for flame1 (ethylene). The comparisons for A2 (Fig. 12a) show the benefit of the additional growth pathways to A2 that are included in the present mechanism. The other two mechanisms underpredict the measured A2 concentrations by about one order of magnitude with the mechanism of Appel et al. [8] and two orders of magnitude with the mechanism of Marinov et al. [11]. A similar result is seen for A2R5, where computations with the present mechanism predict the same order of magnitude as the experiment (although the peak is predicted to be a factor of

two higher) and the other two mechanisms significantly underpredict the measured data. With P2, the situation is similar as all three mechanisms underpredict the measured data, although the underprediction is less severe with the present mechanism. Nonetheless, the present mechanism underpredicts the measured data by about an order of magnitude. The P2 chemistry therefore remains an open area of investigation.

Fig. 12d compares indene concentrations predicted by the present mechanism and by the Marinov et al. [11] mechanism. (Indene is not included in the Appel et al. [8] mechanism.) The results for indene are quite promising as the present mechanism is able to predict the correct order of magnitude of the peak concentrations – a marked improvement on the results of the Marinov et al. [11] mechanism. This is an important result, because as Marinov et al. [11] point out, indenyl/cyclopentadienyl combination is an important route to A3 formation in many combustion systems.

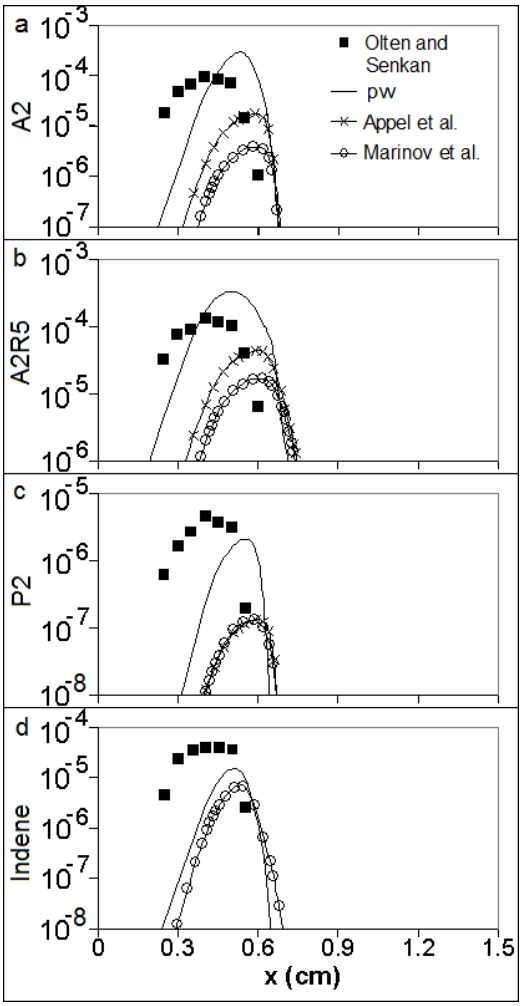

Fig. 12. Comparison of experimental (from [32]) and numerical profiles of aromatics and substituted aromatics for two-ring PAHs for the C_2H_4/air diffusion flame (flame1); a) naphthalene (A2) computed with all three chemical kinetic mechanisms, b) acenaphthalene (A2R5) computed with all three chemical kinetic mechanisms, c) biphenyl (P2) computed with all three chemical kinetic mechanisms, and d) indene computed with the present mechanism and the mechanism of Marinov et al. [11] only (indene is not included in the mechanism of Appel et al. [8]).

The two-ringed species are also compared for flame2 (ethane) in Fig. 13, however, P2 is omitted as it was not included in the experimental dataset of Vincitore and Senkan [33]. Again, there are open questions related to this experimental dataset as evidenced by the unphysical shape of the profiles for A2R5 and indene. Therefore, the experimental data are only taken as approximate, but are useful to judge the correct order of magnitude nonetheless. The predicted A2 profiles with the mechanisms of Appel et al. [8] and Marinov et al. [11] lay coincident and both underpredict the measured values. By contrast, the predicted A2 profile with the present mechanism slightly overpredicts the measured profile. A similar result can be seen for A2R5, but here the overprediction is more severe. The magnitude of the peak indene concentration is reproduced well with the present mechanism and overpredicted by more than an order of magnitude with the Marinov et al. [11] mechanism. This is somewhat surprising since Marinov et al. [11] underpredicted indene for flame1 (ethylene). The reason for this is related to the overprediction of $A1CH_3$ in flame2, the ethane flame (see Fig. 11d) that was seen when the Marinov et al. [11] mechanism was used, which was not present in flame1. In the multi-channel indene formation model developed in the present mechanism, (unlike in mono-channel indene formation), indene grows directly from acetylene addition to $A1CH_2$. The ability of the present mechanism to accurately characterize this process in flame1 and flame2 shows an improvement over the Marinov et al. [11] mechanism.

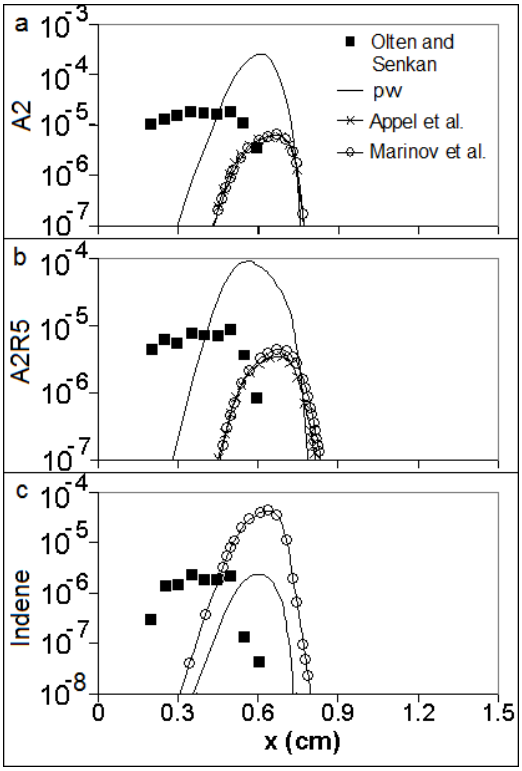

Fig. 13. Comparison of experimental (from [33]) and numerical profiles of aromatics and substituted aromatics for two-ring PAHs for the C_2H_6/air diffusion flame (flame2); a) naphthalene (A2) computed with all three chemical kinetic mechanisms, b) acenaphthalene (A2R5) computed with all three chemical kinetic mechanisms, c) indene computed with the present mechanism and the mechanism of Marinov et al. [11] only (indene is not included in the mechanism of Appel et al. [8]).

Finally, comparisons are made for A3 and A4 between all three mechanisms and the experimental data in Fig. 14 for flame1 (ethylene), and in Fig. 15 for flame2 (ethane). It can be seen from Fig. 14 that the present mechanism is the only one of the three to accurately capture the shape and

order of magnitude of the A3 and A4 profiles, although the shift of the experimental data toward the fuel port still exists. For A3 (Fig. 14a), the two mechanisms from the literature lead to underprediction of concentrations by an order of magnitude. For A4 (Fig. 14b) the situation is worse. The Appel et al. [8] mechanism underpredicts the experimental data by one to two orders of magnitude, and the Marinov et al. [11] mechanism underpredicts by two to three orders of magnitude. This is a crucial result in the validation process of the present mechanism as A3 and A4 are known to be important soot nucleation precursors. With an eye toward coupling the present mechanism to soot formation models in diffusion flames, it is important to be able to accurately model aromatic growth up to A3 and A4. Fig. 14 shows significant improvement of the present mechanism over those in the literature. Since no particle phase model was included in the simulation, the effect of removal of PAHs from the gas phase via particle formation is not accounted for. However, most PAH concentrations peak between 10 and 1000 ppm, while soot concentrations for these fuels and stoichiometry are on the order of 1 ppm. Therefore, this effect would be negligible. For further information, the reader is directed to [31].

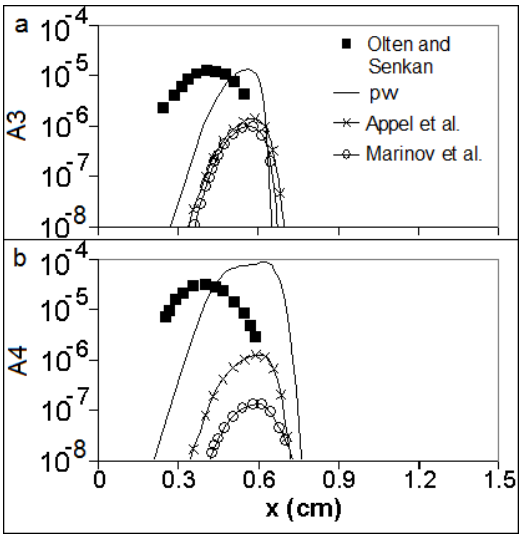

Fig. 14. Comparison of experimental (from [32]) and numerical profiles (computed with all three mechanisms) of aromatic species for the C_2H_4/air diffusion flame (flame1); a) phenanthrene (A3) and, b) pyrene (A4).

The unphysical nature and questionability of some of the data in the Vincitore and Senkan [33] dataset is most evident in Fig. 15a. A3 in the Vincitore and Senkan [33] dataset peaks at x = 0.25 cm from the fuel port, but judging from the A2, A2R5, and indene profiles in Fig. 13, the expected peak location would be between x = 0.45 cm and x = 0.6 cm from the fuel port. Again, the experimental data for A3 and A4 from Vincitore and Senkan [33] should be taken as an estimate of the order of magnitude only. Nonetheless, Fig. 15 also shows that only the present mechanism is able to predict the same order of magnitude seen in the experiments for A3 and A4. For A3 (Fig. 15a) the Marinov et al. [11] mechanism does a relatively good job in predicting the measured order of magnitude and the Appel et al. [8] mechanism underpredicts the experimental data by about one order of magnitude. As for flame1 (ethylene), only the present mechanism is able to predict the correct order of magnitude for A4 (Fig. 15b), again suggesting the greater potential for the present mechanism to be coupled to a soot model and to generate accurate results.

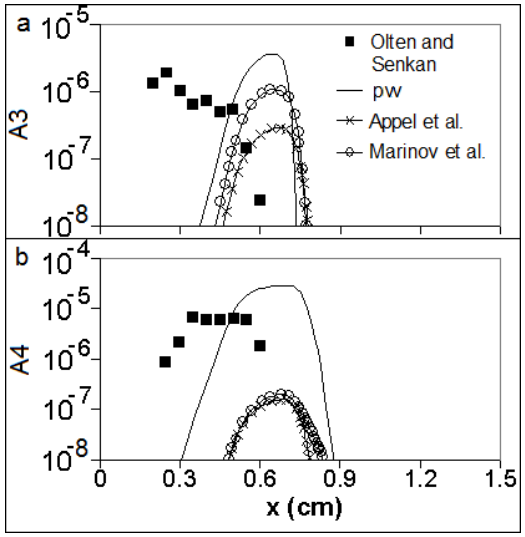

Fig. 15. Comparison of experimental (from [33]) and numerical profiles (computed with all three mechanisms) of aromatic species for the C_2H_6/air diffusion flame (flame2); a) phenanthrene (A3) and, b) pyrene (A4).

4.3 Sensitivity and reaction pathway analysis

Based on a sensitivity analysis and on comparing the relative rates of aromatic production from dominant growth reactions, the relative importance of various aromatic formation pathways in the region of the flame with the fastest aromatic growth can be assessed for each of the three mechanisms. To help explain the differences in A1 formation, these analyses were performed for flame1 (ethylene), and the major A1 formation pathways for each mechanism are identified in Table 4 below. For comparison, the reaction rate parameters (reproduced from each mechanism) are also included in the table. The key reactions for A1 formation that are listed in the table were identified as those contributing significantly to either A1 sensitivity or A1 growth in the region of the flame with the maximum A1 growth rate. For each mechanism, the sensitivity and production rate parameters taken from that region were normalized by the maximum value.

Table 4. Dominant A1 formation reactions for flame1 (ethylene).

Present Mechanism	**A (mole-cm-s-K)**	**b**	**E (cal/mole)**	**Sensitivity**	**Rel. Prod. Rate**
i-C_4H_5 + C_2H_2 = A1 + H	1.60E+15	-1.33	5365	1.00	1.00
2C_3H_3 = A1	1.00E+36	-7.2	8414	0.90	0.27
H_2CCCCH + C_2H_3 = A1	3.00E+13	0.0	0	0.00	0.03
Appel et al.					
2C_3H_3 => A1	5.00E+12	0.0	0	1.00	1.00
n-C_4H_5 + C_2H_2 = A1 + H	1.60E+16	-1.3	5400	0.34	0.03
Marinov et al.					
2C_3H_3 = A1	5.56E+20	-2.5	1692	1.00	1.00
H2CCCCH + C_2H_2 = A1-	3.00E+11	0.0	14900	1.00	0.37
CH_2CHCCH_2 + C_2H_2 = A1 + H	5.56E+20	-2.5	1692	0.32	0.05
C_3H_3+aC_3H_5 = fulvene + 2H	3.00E+11	0.0	14900	0.22	0.15

Benzene formation is dominated by a combination of propargyl combination and C_2/C_4 molecule combination, however, the relative importance of the routes, reaction schemes, and reaction rate parameters differ significantly between mechanisms. In the present mechanism, A1 formation is dominated by the reaction: i-C_4H_5 + C_2H_2 = A1 + H. A1 formation is also sensitive to the propargyl combination reaction: $2C_3H_3$ = A1, however, the relative production rate of A1 from this reaction is only 27%. A1 formation in the present mechanism is insensitive to the reaction: H_2CCCCH + C_2H_3 = A1, from which the relative production rate of A1 is only 3%. By contrast, propargyl combination, which is made irreversible in the mechanism of Appel et al. [8], accounts for the maximum A1 formation sensitivity and the bulk of the A1 production. The only other scheme in Appel et al. [8], leading to any significant A1 formation was the C_2/C_4 reaction: n-C_4H_5 + C_2H_2 = A1 + H with a relative sensitivity of 34%, and a relative production rate of 3%.

In the mechanism of Marinov et al. [11], propargyl combination and the phenyl reaction: H2CCCCH + C_2H_2 = A1- contribute equally to A1 sensitivity, however, much more A1 is produced from the propargyl recombination reaction. This is in contrast to the Appel et al. [8] mechanism, in which only propargyl combination plays a major role in A1 formation, and to the present mechanism, in which the C_2/C_4 reaction: i-C_4H_5 + C_2H_2 = A1 + H is the dominant route. Therefore, the overprediction of A1 formation seen in Fig. 10 may be partly attributable to this reaction. This will remain an area of further investigation.

Two other routes to A1, CH_2CHCCH_2 + C_2H_2 = A1 + H, and the fulvene route: CH_2CHCCH_2 + C_2H_2 = A1 + H, also play a role in the Marinov et al. [11] mechanism. Fulvene goes on to form A1 through hydrogen abstraction reactions analogous to those of phenyl and A1. The overall treatment of A1 formation in Marinov et al. [11] and in the present mechanism are very similar (reversible propargyl combination and various A1- and phenyl-forming C_2/C_4 reactions), however, the different reaction rate parameters account for the disparity in concentration profiles, and varying relative contributions of the reaction schemes.

Similar analyses were performed for A2 formation. The results in Table 5 indicate some similarities in the A2 formation pathways between the present mechanism and the mechanism of Appel et al. [8]. Both mechanisms show a dominant scheme for A2 formation sensitivity involving a single aromatic molecule combining with a C_4 molecule: i-C_4H_5 + A1 → A2+ H_2 + H in the present mechanism, and A1- + C_4H_4 = A2 + H in the mechanism of Appel et al. [8]. Additionally, in both mechanisms, the relative production rate of A2 is dominated by acetylene addition (via a single reaction of $A1C_2H$- + C_2H_2 in the present mechanism and via three reactions of $A1C_2H$* + C_2H_2 and $A1C_2H$ + C_2H in the mechanism of Appel et al. [8] (considering their additive effect). The present mechanism also has small contributions to A2 formation from the cyclopentadienyl combination reaction: $2C_5H_5$ = A2 + 2H and the acetylene addition reaction: n-C_8H_7 + C_2H_2 = A2 + H. Similarly, the mechanism of Appel et al. [8] has minor contributions to A2 formation (7% and 4%, respectively) from the addition of acetylene to $A1C_2H_3$* and n-$A1C_2H_2$. The key difference between the performance of the two mechanisms is that the maximum *absolute* production rates (not shown) of A2 with the present mechanism are one order of magnitude higher than with the mechanism of Appel et al. [8], resulting in the higher A2 concentrations and better agreement with the experimental data seen in Fig. 12. This is attributable to the different reaction rates used in the two mechanisms. Maximum *absolute* production rates of A2 with the Marinov et al. [11] mechanism were two orders of magnitude lower than those of the present mechanism, due to its less complete reaction scheme.

Table 5. Dominant A2 formation reactions for flame1 (ethylene).

Present Mechanism	**A (mole-cm-s-K)**	**b**	**E (cal/mole)**	**Sensitivity**	**Rel. Prod. Rate**
i-C_4H_5 + A1 => A2 + H_2 + H	1.00E+12	0.0	2988	1.00	0.61
A1C_2H- + C_2H_2 = A2-	4.00E+13	0.0	10135	0.14	1.00
2C_5H_5 = A2 + 2H	8.30E+13	0.0	9714	0.00	0.01
n-C_8H_7 + C_2H_2 = A2 + H	1.60E+16	-1.3	5365	0.00	0.01
Appel et al.					
A1- + C_4H_4 = A2 + H	3.30E+33	-5.7	25500	1.00	1.00
A1C_2H* + C_2H_2 = A2-1	2.20E+62	-14.6	33100	0.31	0.58
A1C_2H* + C_2H_2 = A1$C_2H)_2$ + H	1.80E+19	-1.7	18800	0.16	0.80
A1C_2H + C_2H = A1$C_2H)_2$ + H	5.00E+13	0.0	0	0.14	0.70
A1C_2H_3* + C_2H_2 = A2 + H	1.60E+16	-1.3	6600	0.00	0.07
n-A1C_2H_2 + C_2H_2 = A2 + H	1.60E+16	-1.3	5400	0.00	0.04
Marinov et al.					
$C_6H_4C_2H$ + C_2H_2 = A2-	1.07E+04	2.3	-657.3	1.00	1.00
2C_5H_5 = A2 + 2H	2.00E+13	0.0	8000	0.90	0.25

In contrast to the present mechanism, and that of Appel et al. [8], in which A1/C_4-molecule combination play important roles, A2 formation was not found to be sensitive to any reactions involving the first aromatic ring in the Marinov et al. [11] mechanism. Instead, the acetylene HACA reaction, $C_6H_4C_2H$ + C_2H_2 = A2-, and the cyclopentadienyl combination reaction, 2C_5H_5 = A2 + 2H, dominated A2 formation with comparable sensitivities. The cyclopentadienyl combination route only contributed to A2 production with a relative production rate of 25%, but this is significantly greater than the 1% contribution in the present mechanism.

Formation of the third aromatic ring, A3 was also analysed, and the sensitivity and net production rate results are shown in Table 6. Here, the performance of the three reaction mechanisms are quite different. The Appel et al. [8] mechanism forms A3 via comparable contributions from A2- (both isomers, A2-1 and A2-2) combination with C_4H_4, phenyl or benzene combination with A1C_2H or A1C_2H*, respectively, and acetylene addition to P2-. The present mechanism considers all of the aforementioned routes, each of which contribute to A3 formation (although the relative production from A2-/C_4-molecule combination is about four times that of A1C_2H/A1- combination in the present mechanism, and only about twice that of A1C_2H/A1- combination in the Appel et al. [8] mechanism. The Marinov et al. [11] mechanism forms A3 primarily via indenyl combination with cyclopendadiene, which is also included in the present mechanism but only accounts for 2% of the relative production rate.

In addition to the A2-/C_4-molecule combination reaction, the reaction of acetylene addition to A2R5 contributes significantly to A3 in the present mechanism only, which predicts A3 concentrations an order of magnitude higher than with the other two mechanisms. The maximum *absolute* A3 production rates (not shown) in the present mechanism were found to be one order of magnitude higher than in the other two mechanisms (likely caused by the higher A2 concentrations), resulting in A3 concentrations that were in line with the experimental data (see Fig. 14 and Fig. 15).

Table 6. Dominant A3 formation reactions for flame1 (ethylene).

Present Mechanism	**A (mole-cm-s-K)**	**b**	**E (cal/mole)**	**Sensitivity**	**Rel. Prod. Rate**
A2R5 + C_2H_2 => A3	2.77E+04	2.5	29084	1.00	0.41
A2- + C_4H_2 = A3-	3.30E+33	-5.7	25337	0.84	1.00
A1C_2H + A1- = A3 + H	1.10E+23	-2.9	15917	0.44	0.25
indenyl + C_5H_5 => A3 + 2H	4.30E+13	0.0	9714	0.11	0.02
A1C_2H- + A1 = A3 + H	1.10E+23	-2.9	15917	0.00	0.05
Appel et al.					
A2-1 + C_4H_4 = A3 + H	3.30E+33	-5.7	25500	1.00	1.00
A2-2 + C_4H_4 = A3 + H	3.30E+33	-5.7	25500	0.92	0.97
A1- + A1C_2H = A3 + H	1.10E+23	-2.9	15890	0.56	0.90
P2- + C_2H_2 = A3 + H	4.60E+06	2.0	7300	0.00	0.67
A1 + A1C_2H* = A3 + H	1.10E+23	-2.9	15890	0.00	0.23
Marinov et al.					
indenyl + C_5H_5 = A3 + 2H	1.00E+13	0.0	8000	1.00	1.00

The results of the sensitivity and relative production rate analyses for A4 formation are shown in Table 7 below. With the present mechanism, the concentration of A4 is only sensitive to a single formation pathway: A2R5 + C_4H_2 => A4. However, two other routes contribute significantly to A4 production; the acetylene addition route: A3- + C_2H_2 = A4 + H, and the aromatic combination route: A1C_2H- + A1C_2H = A4 + H. With the other two mechanisms, it is only the acetylene HACA reaction A3- + C_2H_2 = A4 + H that contributes to A4 formation (with different isomers of A3- dominating in the two schemes). By contrast, the A3- + C_2H_2 reaction is only responsible for 76% of the production of A4 that is yielded from the reaction of A2R5 with C_4H_2 with the present mechanism. This alternative formation pathway, coupled with the larger A3 concentrations accounts for the higher concentrations of A4 that are seen when the present mechanism is used, which are in good agreement with the experimental data (see Fig. 14 and Fig. 15).

With the present mechanism, the additional A4 formation routes contribute to the good agreement seen for A4. In the two mechanisms in the literature, only HACA addition is used to characterize growth from A3 to A4. As a result, their underprediction gets worse with increasing aromatic rings (see, for example, Fig. 14). In Fig. 14, the underprediction for A3 is only one order of magnitude but for A4, it is two to three orders of magnitude. It is only with the more complete PAH growth submodel in the present mechanism that the comparison does not degrade with increasing aromatic rings.

Table 7. Dominant A4 formation reactions for flame1 (ethylene).

Present Mechanism	**A (mole-cm-s-K)**	**b**	**E (cal/mole)**	**Sensitivity**	**Rel. Prod. Rate**
A2R5 + C_4H_2 => A4	2.41E+02	2.2	-1131	1.00	1.00
A3- + C_2H_2 = A4 + H	6.60E+24	-3.4	17686	0.00	0.76
A1C_2H- + A1C_2H = A4 + H	1.10E+24	-2.9	15917	0.00	0.27
Appel et al.					
A3-4 + C_2H_2 = A4 + H	6.60E+24	-3.4	17800	1.00	1.00
Marinov et al.					
A3-1 + C_2H_2 = A4 + H	3.49E+10	0.6	5658	1.00	1.00

5. Summary and Conclusions

A chemical kinetic mechanism of C_2 fuel combustion and PAH formation and growth has been updated and adapted for use in diffusion flame systems. The mechanism was published in an earlier form and had been validated for one-dimensional laminar premixed methane and ethylene flames. Since that time, a set of reactions, presented in the mechanism described in [31] have been updated to reflect the latest literature data and to reduce numerical stiffness (mostly by modifying low-temperature and reverse reaction rates). In the present study, the mechanism has been used with the OPPDIF code of the CHEMKIN modeling package to simulate two laminar diffusion flames; one that burns ethylene and has been studied experimentally by Olten and Senkan [32], and one that burns ethane and has been studied experimentally by Vincitore and Senkan [33]. These two flames were of particular interest because Senkan and coworkers [32,33] included numerous one- to four-ring aromatic species in their experimental datasets. For further comparison, the same two flames were also simulated using two commonly used chemical kinetic mechanisms from the literature (Appel et al. [8] and Marinov et al. [11]).

Each of the three mechanisms was able to compute major species profiles in both the ethylene and ethane flames. However, it was aromatic species that were of principal interest in the present work. Comparisons were made for A1 and three of its substituted aromatics, A1C_2H, A1C_2H_3, and A1CH_3. For these four species the present mechanism led to slight overprediction of concentration profiles while A1, A1C_2H, and A1C_2H_3 concentrations were reproduced well with the other two mechanisms from the literature. The Marinov et al. [11] mechanism underpredicted concentrations of A1CH_3, which was not included in the Appel et al. [8] mechanism. When both the ethylene and ethane flames were considered, the Appel et al. [8] mechanism performed the best with regard to the first aromatic ring and its substituted aromatics. This discrepancy will remain an open area of further investigation – primarily, the oxidation reactions of A1C_2H, A1C_2H_3, and A1CH_3 have to be analysed, although some of the overprediction may be attributable to the multispecies representation of A1 in the present mechanism. Comparisons of the experimental data and computed profiles made for A2, A2R5, P2, and indene demonstrated that the present mechanism is significantly better than either of the two mechanisms from the literature at predicting the order of magnitude of two-ring aromatic and substituted aromatic concentrations. Concentrations of A2, A2R5, and indene were predicted well by the present mechanism and significantly underpredicted by the two mechanisms from the literature. Here, the benefits of the updates to A2 formation that are considered in the present mechanism, outlined in Slavinskaya and Frank [31] and in Section 2.2 are evident. P2 concentrations were underpredicted by all three mechanisms, but the discrepancy was much less severe with the present mechanism. In predicting A3 and A4 concentrations, the present mechanism showed significant benefit when compared to the two

mechanisms in the literature. The Appel et al. [8] and Marinov et al. [11] mechanisms both underpredicted A3 and A4 concentrations by an order of magnitude or more, whereas the present mechanism reproduced the measured values relatively well.

Sensitivity and production rate analyses were performed in the region of the flame of maximum aromatic formation to identify the dominant A1 formation reactions within each mechanism. It was found that C_2H_2 addition via HACA dominated A1 formation in the present mechanism and propargyl recombination made a smaller but significant contribution. By contrast, in the Appel et al. [8] and Marinov et al. [11] mechanisms, propargyl recombination was the dominant route to A1 formation. The Marinov et al. [11] mechanism also considers a fulvene route to A1, which was found to contribute to A1 formation. Analysis revealed significant differences in the formation of A2 within the three mechanisms. The reaction schemes for A2 formation in both the present mechanism and the mechanism of Appel et al. [8] are comparable, but the reaction rates are very different. As a result, the production rate of A2 with the present mechanism was an order of magnitude higher with the present mechanism. The A2 formation pathways with the Marinov et al. [11] mechanism were comparatively incomplete and resulted in A2 formation rates that were two orders of magnitude lower than with the present mechanism. The dominant routes to A3 formation in the present mechanism were similar to those of the Appel et al. [8] mechanism; C_4 combination with naphthalenyl radical and $A1C_2H$ combination with phenyl. The differences in A3 formation between the two mechanisms were the importance of the irreversible reaction of A2R5 with acetylene in the present mechanism, and the acetylene addition to P2- in the Appel et al. [8] mechanism. A3 formation was very different in the Marinov et al. [11] mechanism, being dominated by cyclopentadienyl/indenyl combination. The importance of A2R5 in the present mechanism was further highlighted as A4 formation was dominated by the irreversible combination of A2R5 with C_4H_2 whereas A4 is formed only by HACA in the two mechanisms from the literature.

The present mechanism, recently updated and adapted for diffusion flame systems, is highly successful at predicting concentrations of aromatics containing two to four rings. Correct order of magnitude prediction was achieved with the present mechanism, marking a significant improvement on commonly used mechanisms in the literature. As these aromatic species are precursors to soot formation and growth, their accurate prediction remains an important goal of combustion research. Unlike previous mechanisms and comparable ones available in the literature, the present mechanism contains a complete set of PAH growth reactions up to Benzo(a)pyrene, determined with a minimal number of fit parameters. When chemical lumping has been unavoidable, atomic fluxes have been carefully maintained. As a result, predicted PAH concentrations are much more in line with experimental data than those from other mechanisms in the literature. When this mechanism is coupled to a soot model, coupling to the PAH gas phase, which is the starting point for soot formation, will be much more accurate. Coupling this mechanism to a particle phase model remains the focus of ongoing investigations.

Supplemental Material

The present chemical kinetic reaction mechanism, thermodynamic data, and transport data are available from the authors (nadja.slavinskaya@dlr.de) upon request as supplemental material.

Acknowledgements

The authors acknowledge the Natural Sciences and Engineering Research Council of Canada and the Ontario Ministry of Research and Innovation for financial support. The authors would like to thank Prof. Tianfeng Lu at the University of Connecticut for his assistance in identifying reaction rates

in the chemical kinetic mechanism that cause numerical stiffness. The authors would also like to thank Dr. Peter Frank from the German Aerospace Center (DLR) for guidance and support, and Prof Alexander Burcat from the Technion - Israel Inst. of Technology for helpful discussions relating to thermodynamic properties.

References

1 S. Vedal, J. Air Waste Manage. Assoc. 47 (1997) 551–581.
2 K.H. Homann, Proc. Combust. Inst. 20 (1984) 857-870.
3 H. Bockhorn, (ed.), Soot Formation in Combustion: Mechanisms and Models, Springer-Verlag, Berlin, 1994.
4 E. Ranzi, Energ. Fuel. 20 (2006) 1024-1032.
5 M. Frenklach, H. Wang, Proc. Combust. Inst. 23 (1990) 1559-1566.
6 M. Frenklach, Proc. Combust. Inst. 26 (1996) 2285-2293.
7 H. Wang, M. Frenklach, Combust. Flame 110 (1997) 173-221.
8 J. Appel, H. Bockhorn, M. Frenklach, Combust. Flame 121 (2000) 122-136.
9 M. Balthasar, M. Frenklach, Combust. Flame, 140 (2005) 130-145.
10 N.M. Marinov, W.J. Pitz, C.K. Westbrook, M.J. Castaldi, S.M. Senkan, Combust. Sci. Technol., 116 (1996) 211-287.
11 N.M. Marinov, W.J. Pitz, C.K. Westbrook, A.M. Vincitore, M.J. Castaldi, S.M. Senkan, Combust. Flame, 114 (1998) 192-213.
12 A. D'Anna, A. D'Alessio, J.H. Kent (cited as J. Kent), Combust. Flame, 125 (2001) 1196-1206.
13 A. D'Anna, J.H. Kent, Combust. Flame, 132 (2003) 715-722.
14 A. D'Anna, J.H. Kent, Combust. Flame, 144 (2006) 249-260.
15 A. D'Anna, J.H. Kent, R.J. Santoro, Combust. Sci. Technol., 179 (2007) 355-369.
16 A. D'Anna, J.H. Kent, Combust. Flame, 121 (2000) 575-592.
17 C.S. McEnally, L.D. Pfefferle, Combust. Flame, 152 (2008) 573-587.
18 R.J. Santoro, H.G. Semerjian, R.A. Dobbins, Combust. Flame, 51, (1983) 203-218.
19 A. D'Anna, A. Violi, Proc. Combust. Inst. 27 (1998) 425-433.
20 A. Violi, A. D'Anna, A. D'Alessio, Chem. Eng. Sci., 54 (1999) 3433-3442.
21 A. D'Anna, A. D'Alessio, A. Violi, Combust. Flame, 121 (2000) 418-429.
22 A. D'Anna, A. Violi, A. D'Alessio A.F. Sarofim, Combust. Flame, 127 (2001) 1995-2003.
23 A. Violi, A. D'Anna, A. D'Alessio, A.F. Sarofim, Chemosphere, 51 (2003) 1047-1054.
24 A. D'Anna, A. Violi, Energy Fuels 19 (2005) 79-86.
25 A. D'Anna, J.H. Kent, Combust. Flame, 152 (2008) 573-587.
26 A. D'Anna, M. Commodo, M. Sirignano, P. Minutolo, R. Pagliara, Proc. Combust. Inst., 32 (2009) 793-801.
27 G.P. Smith, D.M. Golden, M. Frenklach, N.W. Moriarty, B. Eiteneer, M. Goldenberg, C.T. Bowman, R.K. Hanson, S. Song, J. William C. Gardiner, V.V. Lissianski, Z. Qin, GRI-Mech 3.0, http://www.me.berkeley.edu/gri_mech/.
28 H. Böhm, H. Jander, D. Tanke, Proc. Combust. Inst., 27 (1998) 1605-1612.
29 H. Böhm, H. Jander, Phys. Chem. Chem. Phys., 1 (1999) 3775-3781.
30 H. Böhm, K. Kohse-Höinghaus, F. Lacas, C. Rolon, N. Darabiha, S. Candel, Combust. Flame, 124 (2001) 127-136.
31 N.A. Slavinskaya, P. Frank, Combust. Flame, 156 (2009) 1705-1722.
32 N. Olten, S.M Senkan, Combust. Flame, 118 (1999) 500-507.
33 A.M. Vincitore, S.M. Senkan, Combust. Flame, 114 (1998) 259-266.
34 S.B. Dworkin, Q. Zhang, M.J. Thomson, N.A. Slavinskaya, U. Riedel, Combust. Flame, (2011) in press (10.1016/j.combustflame.2011.01.013).
35 K.J. Hughes, T. Turanyi, A.R. Clague, M.J. Pilling, Int. J. Chem. Kinet. 33 (2001) 513-538.
36 I.Gy. Zsély, J. Zádor, T. Turányi, Proc. Combust. Inst. 30 (2005) 1273-1281.
37 D.L. Baulch, C.T. Bowman, C.J. Cobos, R.A. Cox, Th. Just, J.A. Kerr, M.J. Pilling, D. Stocker, J. Troe, W. Tsang, R.W. Walker, J. Warnatz, J. Phys. Chem. Ref. Data 34 (3) (2005) 757.
38 A. Burcat, Ideal Gas Thermodynamic Data in Polynomial form for Combustion and Air Pollution Use, http://www.technion.ac.il/~aer0201/
39 N. A. Slavinskaya "Skeletal mechanism for kerosene combustion with PAH production," AIAA-2008-0992, 46th AIAA Aerospace Sciences Meeting and Exhibit 7-10 Jan 2008, Reno, Nevada (USA).
40 A. Frassoldati, T. Faravelli, E. Ranzi, Int. J. Hydrogen Energ., 32 (2007) 3471-3485.
41 S.P.Karkach, V.I.Osherov, J. Chem. Phys. 110 (1999) 11918-11927.
42 O.P. Shatalov, L.B. Ibraguimova, V.A. Pavlov, G.D.Smekhov, Y.V Tunik, "Analysis of the kinetic data described oxygen-hydrogen mixtures combustion," *4th European Combustion Meeting*, 2009, p. 222.
43 A.D. Isaacson, J. Chem. Phys., 107 (1997) 3831-3839.

44 A.A. Konnov, Russ. J. Phys. Ch. B, 23 (8) (2004) 5-18.
45 C.J. Jachimowski, Combust. Flame, 29 (1977) 55-56.
46 C.J. Brown, G.O. Thomas, Combust. Flame, 117 (1999) 861-870.
47 D.C. Horning, A Study of the High Temperature Autoignition and Thermal Decomposition of Hydrocarbons, Ph.D. thesis, Stanford University,, Stanford, California, USA, 2001.
48 D.M. Kalitan, J.M. Hall, E.L. Petersen, J. Propul. Power, 21 (2005) 1045-1056.
49 S. Saxena, M.S.P. Kahandawala, S.S. Sidhu, Combust. Flame (2010), in press (doi:10.1016/j.combustflame.2010.10.011)
50 X. Zhong, J.W. Bozzelli, Int. J. Chem. Kinet, 29 (1997) 893-913.
51 R.P. Lindstedt, K.A. Rizos, Proc. Combust. Inst., 29 (2002) 2291-2298.
52 L.K. Madden, A.M. Mebel, M.C. Lin, J. Phys. Org. Chem., 9 (1996) 801-810.
53 V.D. Knjazev, I.R. Slagle, J.Phys. Chem. A, 106 (2002) 5613-5617.
54 V.V. Kislov, A.M. Mebel, J. Phys. Chem. A, 111 (2007) 3922-3931.
55 P. Dagaut, G. Pengloan, A. Ristori, Phys. Chem. Chem. Phys., 4 (2002) 1846-1854.
56 C. Cavallotti, S. Mancarella, R. Rota, S. Carra, J. Phys. Chem. A, 111 (2007) 3959-3969.
57 K. Mati, A. Ristori, G. Pengloan, P. Dagaut, Combust. Sci. Technol., 179 (2007) 1261-1285.
58 M.J. Castaldi, N.M. Marinov, C.F. Melius, J. Huang, S.M. Senkan, W.J. Pitz, C.K. Westbrook Proc. Combust. Inst., 26 (1996) 693-702.
59 R.J. Kee, F.M. Rupley, J.A. Miller, et al., CHEMKIN Release 4.1.1, Reaction Design, San Diego, CA, 2007.